

Computational Differential Geometry

Contributions of the Welfenlab to GRK 615

Franz-Erich Wolter, Philipp Blanke, Hannes Thielhelm and Alexander Vais

Abstract This chapter presents an overview on contributions of the Welfenlab to GRK 615. Those contributions partial to computational differential geometry include computations of geodesic medial axis, cut locus, geodesic Voronoi diagrams, (“shortest”) geodesics joining two given points, “focal sets and conjugate loci” in Riemannian manifolds and the application of the medial axis on metal forming simulation. The chapter includes also the computation of Laplace spectra of surfaces, solids and images and the application of those Laplace spectra to recognize the respective objects in large collections of surfaces, solids and images. Beyond that this article touches also on the origin of the afore-mentioned works including research done at the Welfenlab as well as works that can be traced back to the graduate studies of the first author.

1 Introduction

The occasion of writing a report on the contributions of the Welfenlab to GRK 615 gives the first author of this article an opportunity to look back to those years when many of his research projects related to the above-mentioned contributions had its origin. Those were the years of F.-E. Wolter’s own graduate studies in Berlin in the late seventies and early eighties of the last century. There was a time in the 1970s when research on the Riemannian Laplacian operator and its eigenvalues was extremely popular in global differential geometry even more than today. In those days, many members in the community of differential geometry still had in their ears Lipman Bers’ tersely formulated question “Can one hear the shape of a drum?”

In other words, is the shape of a two-dimensional bounded region determined by the eigenvalues of its corresponding Laplacian operator?

Franz-Erich Wolter · Philipp Blanke · Hannes Thielhelm · Alexander Vais
Division of Computer Graphics, Leibniz Universität Hannover, Welfengarten 1, 30165 Hannover, Germany; e-mail: {few, blanke, thielhel, vais}@welfenlab.de

Indeed it was to a significant extent this question and the partly available theoretical knowledge in those days that motivated Wolter early on in the eighties to consider it being an exciting project to investigate via numerical experiments *if Laplace spectra could be employed to define feature vectors that could be used as fingerprints to practically distinguish different objects in large collections of similar surfaces and solids*. That exciting project had to wait until around 1997 when there was a chance to pursue it at the Welfenlab that had been built up by the first author in 1995 when he came to the University of Hannover. It was in 1997 when he asked two students, Herbst and Sust, to present two seminars at the Welfenlab dealing with Gordon's examples of 1992 [17] and (the respective theoretical background) showing the existence of planar polygonal regions that are isospectral but not congruent. This was the starting point for a series of diploma theses investigating Laplace spectra of planar regions; see [3, 20] for curved surfaces aiming at distinguishing those geometric entities by their Laplace spectra. This work was taken up again in 2000 by Peinecke and Reuter studying in their respective diploma theses how Laplace spectra could be used to classify geometric entities like planar domains and surfaces while Peinecke studied the respective problem for images. Peinecke and Reuter became "Kollegiaten" in the GRK 615. Their diploma and especially their PhD research extending and deepening their diploma research built up one important line of research partial to the area of computational differential geometry contributed by the Welfenlab to the GRK 615. We will give more details on this work in Section 4.

In the years of Wolter's graduate research the aforementioned popularity of research on Laplacian spectra was not shared by research related to the Riemannian cut locus – a subject that finally became the center of Wolter's PhD research [45]. The latter research works probably had its origin in Wolter's unsupervised studies on geodesics as presented in the book *Variational Theory of Geodesics* by Postnikov [33]. This book contains an error on page 101, stating there that the squared Riemannian distance function with respect to any given reference point p is differentiable everywhere on a complete Riemannian manifold M . In fact the latter squared distance function $d^2(p, x)$ is not differentiable in a dense subset $Se(p)$ of the cut locus $C(p)$ of p , implying that a complete Riemannian manifold must be diffeomorphic to \mathbb{R}^n in case there exists one point p on M such that the squared distance function $d^2(p, x)$ is differentiable on all M . Here $Se(p)$ contains those points in $C(p)$ having at least two distinct shortest geodesic joins to p . Those results firstly observed by Wolter [44] subsequently lead to new characterizations of the cut locus in terms of differentiability properties of the distance function. In his diploma thesis [43], Wolter looked into the problem of generalizing classical geodesics in Riemannian manifolds to geodesics in bordered Riemannian manifolds. Here the geodesics being locally shortest paths joining any two points in the manifold may have contact with its boundary but must stay inside the manifold. Like in the classical case, the intrinsic distance of any two given points in the bordered manifold may be defined as infimum of lengths of continuously differentiable paths joining the two given points. It turns out that various basic concepts like distance functions and cut loci may be transferred into the situation of bordered manifolds as well. However, there occur new phenomena and new complications as shortest paths in bordered mani-

folds may bifurcate at boundary points. This implies that initial direction and length will not determine uniquely the end point of the geodesic related to the respective start point. Clearly, this causes difficulties for efforts aiming at defining generalizations of classical exponential maps used to control the paths of geodesics.

All those works may be seen as partial to a new approach studying global and local relations between the shape of bordered and unbordered Riemannian geometric objects and its respective intrinsic distance geometry. Here, shape would include topological properties as well as properties determining the isometry type of a geometric object or even more specifically the congruence type, i.e., the geometry type up to a Euclidean motion. In that sense the theory built via the (Riemannian) medial axis and cut locus serves the purpose of global and local shape cognition, reconstruction and classification. The latter property may be seen as an aspect of shape cognition. Note that research on the shape cognition problem could be viewed as a central goal of the computational efforts pertaining to the studies of spectral geometry done at the Welfenlab that were mentioned in the beginning of this introduction.

All the afore-mentioned works of Wolter prior to 1987 were essentially theoretical considerations and it was in 1988 at Purdue University where Wolter firstly created a software system to be used for computational differential geometry [48]. This research was partial to the ARO (US Army Office of Research) funded “Project Riemann” yielding a software system implemented in C, essentially capable of real time computing and visualizing geodesics and curvature lines on parametrically and implicitly defined surfaces being described by the user in a very flexible way via symbolically defined elementary functions. Most of the software development in Project Riemann was done by undergraduate students supervised by Wolter who explained in a summer course to those students the theoretical background and the algorithms being implemented in the system. It is remarkable that Project Riemann ended up as a state-of-the-art system for the respective computational differential geometry tasks as in those days apparently no competing system existed that could perform those computations in a similar generality.

Later on at MIT starting in early 1989, Wolter pursued research in the area of computational differential geometry with an emphasis on applications related to geometric modeling. In fact Wolter’s contributions in those days may be viewed as efforts to appropriately transfer concepts from local and global classical differential geometry to computational geometry to be used in geometric modeling. *All those works were an effort to establish the new area of computational differential geometry. Such an enterprise was still in the very beginning in the years prior to 1990.*

Although the focus of Wolter’s research on computational differential geometry during his years at MIT (1989–1994) were not those topics that he had pursued in his theoretical thesis works, some basic steps were taken preparing for later works that dealt with computational efforts in the area of the medial axis and its geodesic counterpart. In his diploma and doctoral theses [43,45], Wolter had developed the foundations for the theory of geodesics and cut loci in the general setting of bordered and unbordered Riemannian manifolds with mathematical rigor. Since this technically

involved presentation was difficult to digest for computer scientists and engineers, a condensed version focusing on solids in \mathbb{R}^3 was written as MIT report stemming from December 1991 being later presented as a Sea Grant report in the national Sea Grant Library [46]. This report contains the mathematical foundation for various fundamental results on the medial axis and it explains also the relation between the medial axis and the much older concept of the cut locus.

Two results from [46], stated further down, were the basis for later works at the Welfenlab, as well as in the community pursuing research on the medial axis. Those two results involve the medial axis of a solid.

The first result to be mentioned here is called *topological shape theorem* of the medial axis. It states that the medial axis of a solid with twice continuously differentiable boundary in Euclidean space may be viewed as deformation retract of the solid. This result even holds under weaker regularity assumptions for the solid's boundary. The second basic result is the *shape reconstruction theorem*. It states that any solid can be reconstructed from its medial axis transform. The latter result later on lead to the so-called "medial modeller" useful to efficiently design 3D solids in real time via modifying their medial axis and respective radius function. An early simple prototype of this 3D modeller was presented at the Welfenlab in Howind's diploma thesis in 1998 [19]. A more advanced medial modeller was developed in the diploma thesis of Böttcher in 2004 [11, 50].

The variety of cut locus applications arises from the topological flexibility of the reference set. In case of a solid S , the cut locus or the medial axis transformation provides a compressed representation of S , that allows for intuitive shape modeling [49, 50]. According to the topological shape theorem mentioned above the medial axis itself preserves topological properties of the reference solid. The cut locus of a single point p on a complete Riemannian manifold can be interpreted as the natural glueing seam of charts of geodesic polar coordinates with respect to p and is therefore of natural interest when it comes to distance computations.

More precisely, any compact or complete Riemannian manifold may be obtained by (glueing together) identifying points on the boundary of a disc in the cut locus points C_p of a point p on the manifold. This glueing seam concept holds also for the construction of solids with smooth boundary. In the latter case the interior normal collar whose border is given by the solids boundary and by an offset surface (curve respectively) of the solids boundary is topologically glued as to become the solid. Here the respective glueing seam is defined by the solids medial axis, containing intersections points of segments created by (interior) normals to the solid's boundary.

At the Welfenlab since its foundation in 1994, a whole line of computational differential geometry research was involved with the medial axis, the cut locus and closely related concepts in Riemannian and Euclidean settings. Here, the geodesic medial axis is defined with regard to a bordered n -dimensional Riemannian submanifold S of a complete n -dimensional Riemannian manifold and contains all centers of maximal geodesic balls contained in S .

Medial sets consist of points being equidistancial with respect to two or more reference sets. First computations of medial curves on regions in the Euclidean plane

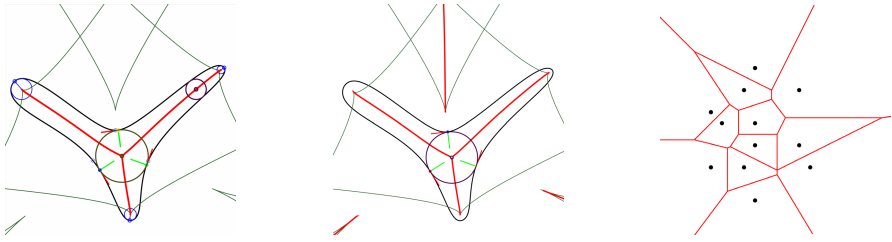


Fig. 1 Medial axis, cut locus and voronoi diagram.

were done by Wolter in 1990 and later on in 1995 on surfaces at the Welfenlab, see [35]. This led to the computation of Voronoi diagrams for points on parametric surfaces by Kunze [22] and the computation of the geodesic (Riemannian) medial axis of bordered subsets of parametric surfaces in Euclidean 3-space [5]. Many results from these works are part of the PhD thesis of Rausch [34]. Funded by the GRK 615, this line of research was later on pursued in Naß' PhD thesis [18] and finally in the still ongoing thesis works of Thielhelm. The ongoing thesis works of Blanke that had been funded by GRK 615 is dealing with applications of the medial axis in two and three dimensions to be used for rapid modeling of metal forming processes. We will present an outline of the latter line of research in Section 3.

2 Medial Sets in Euclidean and Riemannian Spaces

For the purpose of clarity we shall start with a short explanation of the aforementioned geometric concepts.

The *medial axis* $M(S)$ of a reference solid $S \in \mathbb{R}^d$ is defined by the set of all points being centers of maximal balls contained in S . The function $r : M(S) \rightarrow \mathbb{R}_{\geq 0}$ assigning to any medial axis point p the radius of the maximal ball with center p and radius $r(p)$ is called *radius function* of the medial axis. The pair $(M(S), r)$ of medial axis and respective radius function constitutes the *medial axis transform* of a solid.

The *medial set* $MS(A, B)$ of two closed reference sets A, B is the set of all points with equal distance to A and B .

To investigate more general situations it is convenient to introduce the *cut locus* $C(A)$ of a given reference set $A \subseteq \mathbb{R}^d$ as the closure of the set of all points, that have at least two shortest paths to the reference set. In fact, the medial axis can be understood as a special case of the cut locus, since we have $M(S) = C(\partial S) \cap S$, where ∂S denotes the topological border of the solid S [46].

For a discrete and finite set of points $A = \{p_1, \dots, p_n\}$ the cut locus of A is usually referred to as the *Voronoi diagram* of A , which has found numerous applications reaching from geophysics to physiology, that usually base on a distance related partition of \mathbb{R}^d with respect to A .

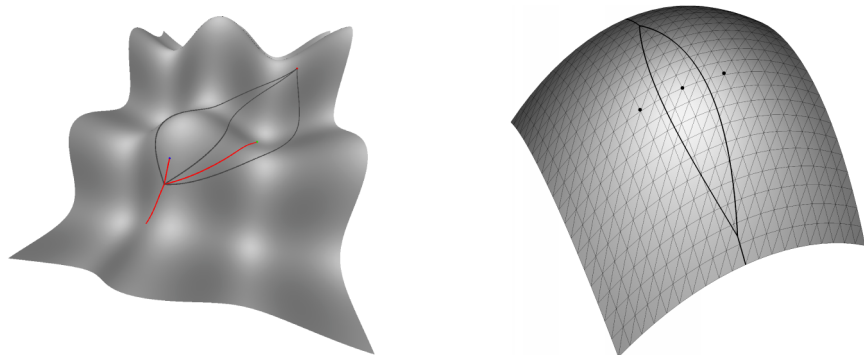


Fig. 2 Complications arising from non-Euclidean situations.

A generalization of the cut locus concept to non-Euclidean spaces M with metric d_M requires the existence of so-called distance realizing paths, which are paths that connect two given points $p, q \in M$ with length $d_M(p, q)$. A special class of metric spaces of natural interest are Riemannian manifolds. A Riemannian manifold is defined as a differentiable manifold M together with a family of metric tensors g_p . Among Riemannian manifolds are those ones of particular importance that are complete as metric spaces. Those spaces are called complete Riemannian manifolds. According to a theorem of Hopf and Rinow a complete Riemannian manifold may also be characterized by the property that every geodesic ray may be extended up to infinity. The above-mentioned theorem of Hopf and Rinow also says that in a complete Riemannian manifold any two given points can be joined by a distance realizing path. Such a path is often called distance minimizer. Uniqueness of minimal geodesic joins however, which holds in the Euclidean case, can not be guaranteed and this leads to significant difficulties in the context of geodesic coordinates and distance computation. We would like to illustrate this with an example shown in Fig. 2. Here the left part shows that on a surface the cut locus of a single point indicated by the red colored set can have a complicated structure while the cut locus of a point in the plane is empty. The right part of Fig. 2 shows that on surfaces a Voronoi diagram (being the cut locus of a finite point set) may contain compact proximity regions bounded by two edges only while in the Euclidean plane a compact proximity region of some point has at least three edges.

To be more precise we shall give some basics on the connection of metric, distance function, metric tensor and the length of curves in n -dimensional Riemannian manifolds M with *metric tensor* $g_p : T_pM \times T_pM \rightarrow \mathbb{R}_{\geq 0}$. Here T_pM denotes the tangent space of a Riemannian manifold M in the point p . In local coordinates the metric tensor g_p can be described by a matrix g_{ij} depending on the (foot) point p of the respective tangent space T_pM . For the sake of simplicity we focus on differentiable curves and refer to [15] or especially [43, 45] for a more detailed introduction and discussion. The length L of a curve $c : [0, 1] \rightarrow M$ is given by

$$L(c) := \int_0^1 \sqrt{g(c'(t), c'(t))} dt,$$

and minimizing over all curves that connect two arbitrary points $p, q \in M$ we obtain a metric space in the sense of point set topology by defining

$$d_M(p, q) := \inf\{L(c) | c(0) = p, c(1) = q\}$$

on M , the so called *Riemannian distance*. The respective minima are called *distance minimizers* or *shortest paths*. To determine the distance for an arbitrary pair of points one obviously has to compute the corresponding distance minimizing path joining the points. Unfortunately it is usually very difficult to compute globally shortest paths.

However, their local counterparts, so-called geodesics, can be computed using the *geodesic differential equations*:

$$\gamma_k''(s) + \sum_{i,j} \Gamma_{ij}^k \gamma_i'(s) \gamma_j'(s) = 0, \tag{1}$$

where the *Christoffel symbols* are the local coefficients of the *Levi-Civita connection*:

$$\Gamma_{ij}^k = \frac{1}{2} \sum_m g^{mk} \left(\frac{\partial}{\partial x_j} g_{im} + \frac{\partial}{\partial x_i} g_{jm} - \frac{\partial}{\partial x_m} g_{ij} \right).$$

Here g^{ij} denotes the inverse of the metric tensor matrix g_{ij} . Note that a (globally) shortest path joining two points is always a geodesic but not vice versa. The descriptions above make use of a local parametrization $X : \mathbb{R}^n \rightarrow M$ of M , that maps the coordinates x_1, \dots, x_n diffeomorphic to M . Here we assume for simplicity that M is a submanifold of \mathbb{R}^k , but the concept holds also within a more general setting. A *geodesic* starting at $p = X(p_1, \dots, p_n) \in M$ with the initial direction $v = DX \cdot (v_1, \dots, v_n) \in T_pM$ is given by $\gamma(s) := X(x(s)) := X(\gamma_1(s), \dots, \gamma_n(s))$, when choosing the initial values of (1) according to $\gamma_k(0) = p_k, \gamma_k'(0) = v_k$.

To simplify the notation we introduce the *exponential map* $\exp_p : T_pM \rightarrow M$ by $\exp_p(v) := \gamma(1)$, i.e. mapping an initial starting direction to a corresponding point $q = \exp_p(v) \in M$. The exponential map enables us to use coordinates of the tangent space T_pM to parametrize M , via so-called *geodesic coordinates*. Using for example polar coordinates (s, φ) , $\varphi = (\varphi_1, \dots, \varphi_{n-1})$ to parametrize T_pM leads to *geodesic polar coordinates* denoted by

$$O_p(s, \varphi) := \exp_p(v(s, \varphi)).$$

O_p is usually referred to as *offset function* of p . Figure 3 shows an example of isolines of geodesic polar coordinates.

For a more complicated reference set, represented by a d -dimensional submanifold $N \subset M$ with local parametrization $\xi : \mathbb{R}^d \rightarrow N$ and coordinates $\xi = (\xi_1, \dots, \xi_d)$, the corresponding offset is given by

$$O_N(\xi, s, \varphi) := \exp_{\xi}(v(s, \varphi)), \tag{2}$$

with $v \in T_p N^\perp$ where the tangent space $T_p M$ splits according to $T_p M = T_p N \oplus T_p N^\perp$ and $\varphi = (\varphi_1, \dots, \varphi_{n-d-1})$.

The offset function O_p and its partial derivative $\partial O_p / \partial s$ is computed by numerically tracing the ODE (1). In the context of distance or medial computations it is also necessary to obtain the partial derivatives with respect to the parameters ξ or φ , i.e. to compute the variation of geodesic coordinates. More generally, consider a one parameter family of geodesics $c : I \times [0, a] \rightarrow M$ where each curve $s \mapsto c_\eta(s) := c(\eta, s)$ is a geodesic. The derivative

$$w(s) := \frac{\partial}{\partial \eta} c(\eta_0, s)$$

defines a vector field along $\gamma := c_{\eta_0}$, which is a so-called *Jacobi field* that satisfies the *Jacobi equation*

$$\frac{D^2}{ds^2} w + R(w, \gamma') \gamma' = 0, \tag{3}$$

where R is the *Riemannian curvature tensor* and D/ds is the *covariant derivative* along γ . For a detailed definition and description of these two central concepts of differential geometry we refer to [15]. The vector field w can be easily decomposed into two components one parallel to the geodesic and the other orthogonal to the geodesic. In the two-dimensional (surface) case the orthogonal component being contained in a one-dimensional subspace of the tangent plane can be described by a real number $y(s)$ at the point $\gamma(s)$ of the geodesic γ . Hence here $y(s)$ describes the oriented length of the Jacobi field, characterizing it completely. The function y satisfies the simplified equation

$$y''(s) + K(\gamma(s))y(s) = 0, \tag{4}$$

with K being the Gaussian curvature along γ . For general n -dimensional Riemannian manifolds solving the Jacobi equation (3) boils down to solving an n -dimensional second order linear system of differential equations along a geodesic γ . This is equivalent to solving a $2n$ -dimensional first order system of differential equations along $\gamma(s)$. Here in addition to the initial values of geodesics (cf. (1)) we need to provide also the initial values of the vector field w . These, however arise from the special form of variation.

Of particular interest are the points where the differential of O_p becomes singular. These points make up the so-called *focal set* of the reference object here being a point p . In this case the focal set of p is also called (first) conjugate locus of p . Within our setting, points located on the focal set (or conjugate locus) of p can be characterized by the condition

$$\det DO_p(s, \varphi) = 0 \text{ with } DO_p = (\partial_s O_p, \partial_\phi O_p) = (\partial_s O_p, y(s)(\partial_s O_p)^\perp),$$

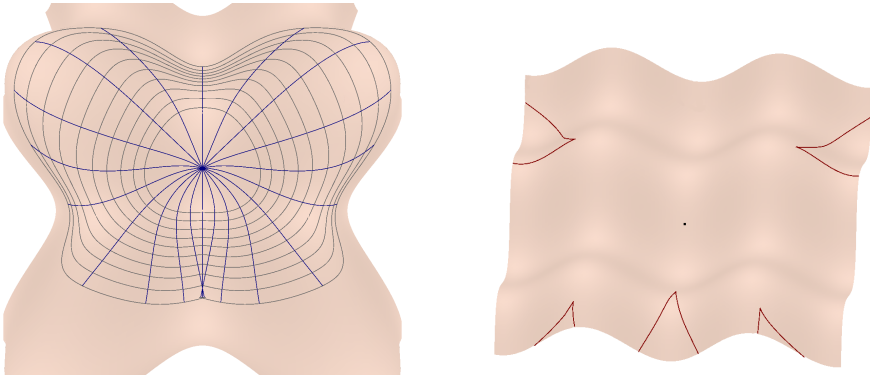


Fig. 3 Geodesics and focal curves.

implying that the focal set of p in two dimensions can be described by the implicit equation $y(s, \varphi) = 0$. We use the latter equation for implicitly describing a focal curve being a (connected) component of the focal set of p and get

$$y(s(t), \varphi(t)) = 0. \tag{5}$$

We want to trace the above-mentioned focal curve by integrating its tangent vector $(s'(t), \varphi'(t))$. The latter may be obtained from equation (5) by differentiating with respect to t and applying the chain rule. Therefore in two dimensions the focal set can be computed by numerically tracing the zero set of y using the implicit differential equation

$$\frac{\partial y}{\partial s} s'(t) + \frac{\partial y}{\partial \varphi} \varphi'(t) = 0$$

That leads to a solution $s(t), \varphi(t)$ which describes the focal set in polar coordinates with respect to p [35]. (The respective detailed computations needed to compute tangent vectors of the focal curve are quite involved. They also employ derivatives of the Gaussian curvature.) An example of resulting focal curves is shown in Fig. 3.

The tools of differential geometry presented above are used to state and solve problems such as the shortest-distance problem or the computation of medial sets in higher dimensional Riemannian manifolds. (For the sake of simplicity we keep the same symbolic notation with $\varphi = (\varphi_1, \dots, \varphi_{n-1})$ now referring to a vectorial parameter.)

For example, to determine the distance of two arbitrary points $p, q \in M$ we can reduce the challenge of finding the shortest path from p to q to computing all geodesics that connect p and q , since every shortest path has to be a geodesic. This translates to finding tuples of geodesic parameters (s^j, φ^j) that satisfy

$$O_p(s^j, \varphi^j) = q. \tag{6}$$

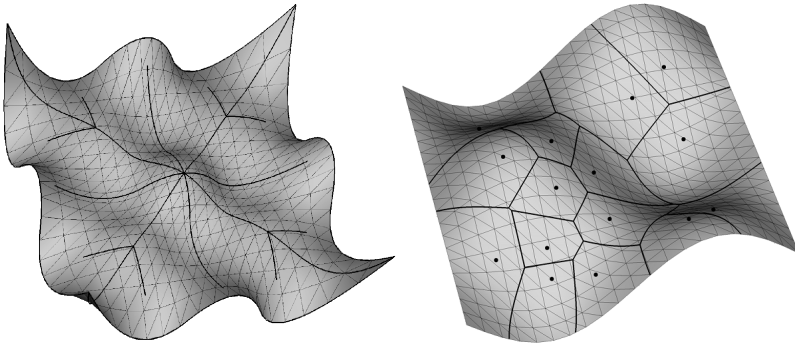


Fig. 4 Medial axis and Voronoi diagram on 2D manifolds ([5, 22, 49]).

This boundary value problem can be looked upon as the problem to solve a nonlinear system of n equations with the n unknowns $s^j, \varphi_1^j, \dots, \varphi_{n-1}^j$.

The computation of the medial set of two reference sets A and B in M translates to finding tuples of geodesic parameters $(\xi, \eta, \varphi, \psi, s)$ that satisfy

$$F(\xi, \eta, \varphi, \psi, s) := O_A(\xi, s, \varphi) - O_B(\eta, s, \psi) = 0,$$

where O_A, O_B are the generalized offset functions defined in (2). By differentiation we obtain a differential equation, called *medial differential equation*, that can be used to trace (isolines) of the medial set. For example, in case A and B are two points and using t as the parameter of a component in the one-dimensional medial set we obtain

$$\left(\frac{\partial O_A}{\partial \varphi} \Big| - \frac{\partial O_B}{\partial \psi} \Big| \frac{\partial O_A}{\partial s} - \frac{\partial O_B}{\partial s} \right) \cdot \frac{d}{dt} \begin{pmatrix} \varphi(t) \\ \psi(t) \\ s(t) \end{pmatrix} = 0$$

In the years between 1996 and 1998/99 the research on computing geodesic medial curves, geodesic medial axes on bordered subsurfaces of spline patches as well as computing geodesic Voronoi diagrams on parametric surfaces had reached some maturity. Among the tools employed for the computation, three basic ingredients stand out. The first one is the so-called geodesic medial differential equation already present in a basic form in [45, pp. 171–174], later on used within a computational setting in [35]. The second one is the computational description of focal curves [35] and the third ingredient, is the observation that on a bordered C^2 -smooth surface assembled from finitely many real analytic surface patches with real analytic boundary arcs, the medial axis would be topologically a graph [49]. The end points of the latter graph would be focal points with respect to the surface's boundary curve [34, 49]. Since the distance between the surface boundary curve and the focal curve has local minima at the end points of the medial axis graph, a tracing method could be implemented starting at those points.

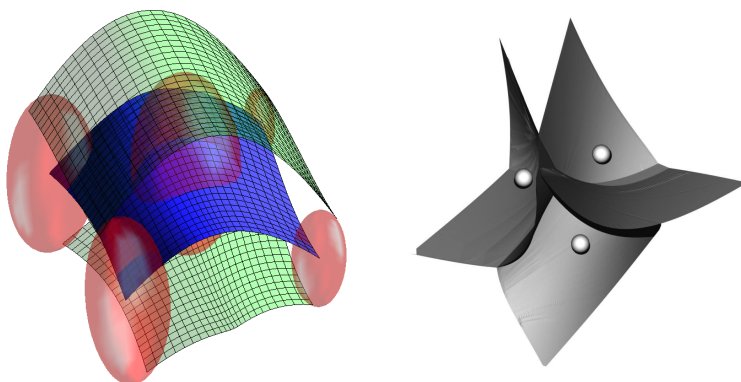


Fig. 5 Medial axis and Voronoi diagram on 3D Riemannian manifolds.

Combining the computational instruments and observations presented above, it was possible to develop prototype software that could compute medial sets in fairly challenging cases of bordered subsurfaces, e.g. spline surfaces or surfaces being C^2 -smoothly assembled of real analytic patches [5,22,34,49]. The tools presented above allow also computing of a Voronoi diagram on a parametric surface [22] provided that the bisectors involved to describe the Voronoi diagram do not meet the focal set of one of the two points defining the bisector (see Fig. 4 for an example). For a more comprehensive survey of the presented research prior to the year 2000, see also [49].

2.1 Medial Computations Since 2000 during the Years of GRK 615

Since the year 2000, the contributions of of the Welfenlab with respect to medial axis computations brought significant extensions beyond that what had been achieved before. This was essentially possible through research works supported by GRK 615.

First, the restriction to two dimensions for the respective computations on geodesic medial sets and geodesic Voronoi diagrams could be removed. Thus, it was possible to develop methods that would work in Riemannian worlds of dimension three and higher and it was possible to present prototypical implementations for the computation of sample cases for medial sets in dimension three. Furthermore, several examples of geodesic Voronoi diagrams of point sets P in Riemannian manifolds of dimension three could be obtained [18, 27, 41] as shown in Fig. 5.

All those computations needed some substantial extensions of the methods that had been developed by the year 2000. For instance, the Jacobi equation had to be solved in its general form (3) instead of its simpler two dimensional special case (4). Another significant extension was caused by the problem that finding a geodesic

joining any two points could not be done any more by a simple shooting method that one might use in dimension two. The additional degrees of freedom in the dimension of the space describing the initial directions made it necessary to employ homotopy methods. For a general introduction to those methods, we refer to [2, 16]. In our case, the nonlinear equation (6) is embedded into a homotopy

$$H(s, \varphi, \lambda) = O_p(s, \varphi) - c(\lambda)$$

where $c : [0, 1] \rightarrow M$ is a curve connecting an arbitrary starting point $c(0)$ with the point $c(1) = q$. Assuming (s, φ, λ) to be a function of an additional parameter t and differentiating with respect to t we obtain the implicit differential equation

$$\left(\frac{\partial O_p}{\partial s} \middle| \frac{\partial O_p}{\partial \varphi} \middle| - c'(\lambda) \right) \cdot \frac{d}{dt} \begin{pmatrix} s(t) \\ \varphi(t) \\ \lambda(t) \end{pmatrix} = 0$$

that can be used to trace the zero set of H whose intersection with the plane $\lambda = 1$ contains the sought solutions. For more details, we refer to [18, 26, 27].

However, all considerations in the years from 1996 to 2007 were focussing on the simplified case, where shortest paths are unique. In elaborated experiments it was discovered that the traced solution paths $x(t) = (s(t), \varphi(t), \lambda(t))$ satisfying $H(x(t)) = 0$ can turn around with respect to λ in points where $\partial O_p / \partial \varphi$ vanishes, i.e. in points where the curve c meets the focal curve of p transversally by construction, see Fig. 6. Therefore if we introduce a generalized homotopy curve c which contains the point q in its interior, the approach can yield multiple solutions. The curve $c(\lambda(\varphi))$ describes end points of a (continuous) family of geodesics starting in p whose initial direction continuously depends on an angle φ . In case there are multiple solutions we obtain for different (initial) angles φ^k the same parameter $\lambda = \lambda(\varphi^k)$ related to geodesics ending up in the same end point $c(\lambda(\varphi^k)) = c(\lambda)$.

In typical situations as depicted in Fig. 6, the focal curve (red-coloured) separates regions of the surface where the number of solutions changes. More concretely we have a unique (geodesic) connection outside of the region bordered by the focal curve (cyan-coloured), two connections on the border (green-coloured) and three connections inside (blue-coloured). The right part of Fig. 6 indicates how to collect different geodesics corresponding to different angular parameters φ and intersecting in the point $c(\lambda)$. Since the structure of focal curves shows some variety, a classification of relevant situations where the number of near by geodesics can be found precisely is subject of ongoing research. In this context the just described method appears to be a promising approach for the computation of “near by” (and under additional assumptions of all) geodesics joining two points $p, q \in M$. Thus the computation of $d_M(p, q)$ is feasible in a direct manner with respect to the definition of d_M . Apparently the latter approach has not been described in the respective literature.

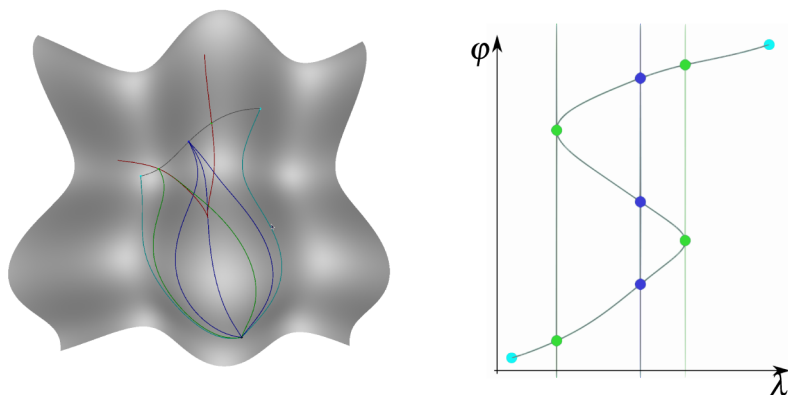


Fig. 6 Several geodesics.

2.2 Remarks

The discussions and methods presented in the preceding section (and also all the underlying respective research until today) make some simplifying assumptions implying the omission of crucial difficulties. Those simplifying assumptions were taken for granted for computations in the two-dimensional surface case or even in the planar case. Therefore in the latter two-dimensional cases important and difficult computational problems related to computations regarding medial axis and Voronoi diagrams in the Riemannian or even in the Euclidean case are still subject of our ongoing research activities. We illustrate this statement with a few examples:

1. For the computation of Voronoi diagrams, the generating point set was assumed to be “benign”, meaning that the related medial sets and bisectors would stay away from the (first) focal sets of their generators.
2. Furthermore, an n -dimensional Riemannian version of the respective Euclidean “general position” assumption was made for the point set generating the Voronoi diagram. This means vertices of the respective geodesic Voronoi diagram were assumed to be centers of uniquely defined geodesic distance spheres containing exactly $n + 1$ generator points partial to the point set generating the Voronoi diagram.
3. The computation of the medial axis close to an end point was usually done by a fairly crude approximation whenever the angle between intersecting geodesic normals became very small close to the respective end point of the medial axis.
4. The analysis of the situation where one wants to compute all geodesics joining a reference point p with points close to the cut locus of p where those geodesics have already or will soon reach the (first) focal locus of p appears to have never been done appropriately in a systematical way. The latter situation is crucial for computing minimal geodesics joining two given points in a complete Riemannian manifold.

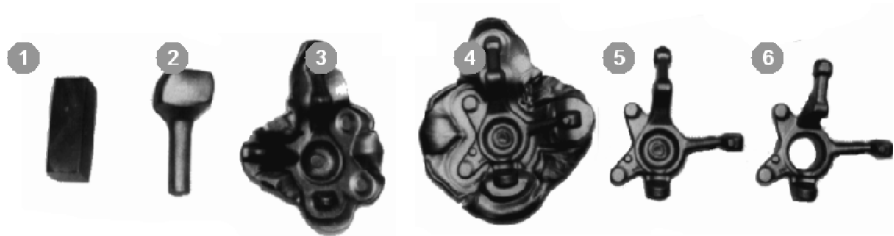


Fig. 7 Sequence of forging steps from billet to final product.

The last two afore-mentioned issues 3 and 4 also fall within the scope of our current research projects.

3 Application of 3D-Medial Axis on Metal Forming Simulation

One application of the medial axis was researched in the graduate college 615, using the medial axis transform as description for the geometry of forging dies in hot drop forging. This serves as basis for rapid backwards simulation of material flow.

In hot metal drop forging, a heated semi-finished part is formed by pressing two forging dies which contain the negative final shape. If the design of the forging dies or the layout of the process is incorrect, the quality of the final product will be severely reduced.

Since the design of the tools is a very cost-intensive part of forging, computer aided techniques are used to reduce design time and to decrease the number of iterations until the final layout is reached. Usually, a number of pre-forms are needed in order to achieve the final complex shape from the initial simple shape with optimal properties and within a geometrical tolerance.

The prediction of preforms from the final product is what we call inverse or “backward” simulation. There exist several approaches, based on the Finite-Element-Method and backward tracking of solutions [9, 21] or upper boundary methods [12]. These algorithms have quite severe drawbacks, since they have to be fitted closely to the problem at hand and have to our knowledge not been utilized in practical applications.

The medial axis approach is based on experimental observations and elementary plasticity theory, see Mathieu et al. [23]. In drop forging experiments, Mathieu noticed that the material flow followed specific paths, which can be described as medial axis of the die gap. Based on Mathieu’s observations, algorithms were developed which simulate material transport along these displacement paths [6, 25]. It is important to note that these simulations only provide an approximation to the velocity field of the material and the filling of the forging form. They will not yield local stresses, strains or temperature, and do not allow the computation of hardening phenomena. Thus, they can provide only limited assistance for the simulation of the

forging process. Nevertheless, this approach is a good basis for backwards simulation where a prediction of the preform is needed as implemented by Wienstroer for the 2D case [42]. The velocity field of the material is not computed explicitly, rather an iterative method based on flow resistance along the displacement paths is used to determine the distribution of material between the cells.

Computation of the Medial Axis for CAD Objects

Forging dies are usually described by surface models constructed in CAD programs, but these programs do not offer a medial axis (MA) representation. Since there exist no production ready programs that offer the construction of the medial axis from (boundary) surfaces, it was necessary to develop a stable tool to this end. Our demands on the algorithm were that it should be fast and return a surface (mesh) representation of the MA. Speed is important because the backward simulation should give the user a first preform which is afterwards analysed and corrected. The simulation will iterate several time steps and in each the MA has to be computed again. Therefore the computation of the MA should be fast. The material transport in the simulation will take place on the MA, so it is crucial that its connection information is obtained. We chose to look for algorithms that take triangle mesh surfaces as input, since the formats of surface representations in CAD tools differ very much, but every system can export triangle meshes, giving us a wide range of possible applications.

Research on existing algorithms showed, that these can be classified into three categories: discrete, direct and indirect methods. Discrete methods discretize the surrounding space of the reference surface using, e.g., octrees or voxels, and then implement a discrete grassfire algorithm (i.e. a thinning operation) to determine a discrete representation of the MA. These methods do not provide the connectivity information and were therefore discarded.

In three dimensions, the MA is composed of medial faces (i.e. bordered surface patches) connected by medial seams (i.e. curve elements). Direct methods setup generalized Voronoi diagrams between elements of the reference surface (triangles) and intersect these to get the medial seams [13,40]. Their runtime is $O(n^2)$ which is bad for large input sets.

The indirect approach approximates the Medial Axis by filtering or pruning the Voronoi diagram of sample points on the reference surface [4, 14]. We have implemented such a strategy, robustly computing a 3D Delaunay tessellation of a sampled point set. Then, we filter the dual Voronoi diagram using a heuristic based on the assumption that there should exist a homeomorphism between the reference surface and the surface Delaunay triangles. Several steps have to be performed prior to the tessellation used to transform the given tool geometry to a boundary representation of the die gap and to analyze its features, e.g., detecting sharp edges. Finally a meshed medial surface of the die gap is computed as shown in Fig. 8.

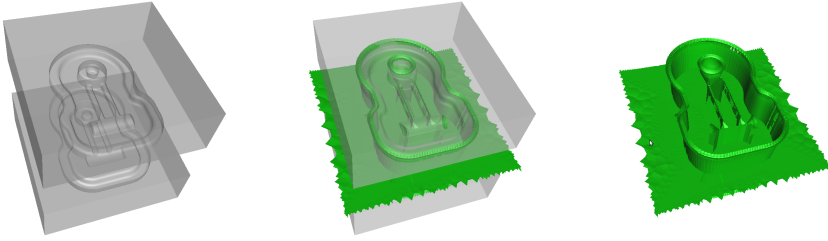


Fig. 8 Forging dies and approximated medial axis of the die gap.

To this end, a fast data structure for the Delaunay triangulation has been implemented by Obydenna [29] and used by Algaier [1] to rapidly recompute the Voronoi diagram after each time step in which the dies move.

Connection between Medial Set and Material Flow

We could show that for viscous Bingham fluids flowing in a completely filled pipe, the maxima of material flow speed will lie on the Medial Axis of the pipe boundary [10]. Hot metal in forging can be modeled as a very viscous Bingham fluid.

Simulation Scheme

With the development of the Medial Axis computation software, the fundament of the simulation has been laid. Important parts of the framework, such as the partition of the die gap and graph-representation of the Medial Axis are already in place. The next steps will be the implementation of the geometric resistance model and the material transport algorithm.

4 Spectrum of Eigenvalues of the Laplace–Beltrami Operator

As pointed out in the introduction, it is known from theoretical research, that a substantial amount of geometric and topological information on a Riemannian Manifold M is contained in the spectrum of eigenvalues of its associated Laplacian. To become more concrete in the following discussion, let M denote a Riemannian manifold and let Δ denote its associated Laplacian. In case M is a subdomain of euclidean space equipped with cartesian coordinates, Δ is the well-known Laplace-Operator given by $\Delta = \sum_i \partial_{ii}$, assigning to a function the trace of the Hessian of that function. In the more general Riemannian setting, this operator becomes the *Laplace–Beltrami-Operator*, whose action on a function f can be defined using the metric tensor g of

M with respect to a local chart via

$$\Delta f := \operatorname{div} \operatorname{grad} f := \frac{1}{\sqrt{\det g}} \sum_{i,j} \partial_i (g^{ij} \sqrt{\det g} \partial_j f)$$

The *spectrum* of M consists of all scalars λ that satisfy the eigenvalue equation

$$-\Delta f = \lambda f \tag{7}$$

for a non-zero function f defined on the manifold, subject to appropriate boundary conditions of the Dirichlet or Neumann type. From the theory of compact elliptic operators it is known, that there is a countably infinite number of non-negative eigenvalues $\lambda_1 \leq \lambda_2 \leq \lambda_3 \leq \dots$ accumulating at infinity. Each eigenvalue corresponds to a finite dimensional space of eigenfunctions.

Among the geometrical information determined by the spectrum we have the dimension and the volume of M , the volume of its boundary, the scalar curvature integral over M , the mean curvature integral over its boundary and the Euler characteristic of M in case of a two-dimensional surface or a planar domain with smooth boundary. This information can be extracted from the asymptotic expansion of the so-called *heat-trace* function

$$Z(t) = \sum_{i=1}^{\infty} \exp(-\lambda_i t) = (4\pi t)^{-\dim M/2} \left(\sum_{i=0}^n c_i t^{i/2} + o(t^{(n+1)/2}) \right) \quad \text{for } t \rightarrow 0^+,$$

where, according to a theorem by McKean and Singer [24], the first few coefficients are given by

$$c_0 = \operatorname{vol} M, \quad c_1 = -\frac{\sqrt{\pi}}{2} \operatorname{vol}(\partial M) \quad \text{and} \quad c_2 = \frac{1}{3} \int_M K - \frac{1}{6} \int_B J \tag{8}$$

where K is the scalar curvature of M and J is the mean curvature of the boundary of M . In case the dimension of M is two, then K coincides with the Gaussian curvature of M .

The spectrum is invariant under isometric transformations of M and changes continuously as the manifold is continuously deformed in a non-isometric way. Therefore the spectrum can be considered to be characteristic for the intrinsic shape of the underlying manifold. However it is also well-known that the spectrum does not completely determine the underlying manifold, as exemplified by the existence of pairs of isospectral but non-isometric manifolds. One such a pair in the case of planar domains was given by Gordon in [17] and is depicted in Fig. 9. An interesting property of these examples is, that isospectrality still holds with respect to the eigenvalues of the three dimensional Laplace operator in case the domains are extruded to three dimensional prisms. However, the boundaries of the prisms have different spectra with respect to their respective two-dimensional Laplace–Beltrami operators.

Leaving aside the rare phenomenon of isospectrality, the above-mentioned theoretical properties of the Laplace spectrum make it suitable for the construction of

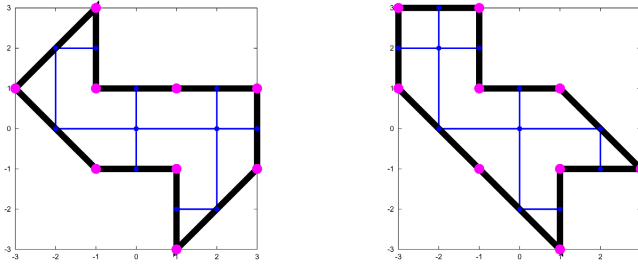


Fig. 9 Isospectral domains.

feature vectors that can be used as *fingerprints* of objects, as long as the objects under consideration can be represented or at least modeled as Riemannian manifolds. The above-mentioned fingerprint can be constructed from a (finite) initial part of the spectrum of the respective manifold and finds a natural application in the context of efficient retrieval of similar objects in large databases.

4.1 Laplace Spectra as Shape DNA for Surfaces and Solids

The two-dimensional surfaces and three-dimensional solids commonly encountered in CAD/CAE applications are instances of Riemannian manifolds with with an intrinsic metric that is naturally induced by their embedding in \mathbb{R}^3 . Extending the work on mesh-based discrete Laplacians, the Laplace–Beltrami Operator can also be applied to free-form surfaces and solids. A collection of its first few smallest eigenvalues can be used as feature vectors that are invariant with respect to rotation and translation and any reparametrization parametrization of the object. Furthermore, it is known that a scaling transformation by the factor a results in scaled eigenvalues by the factor $1/a^2$. Therefore, by normalizing the eigenvalues, shape can be compared regardless of the objects scale.

By transforming the eigenvalue problem (7) into a variational formulation, the Finite Element Method can be employed in order to obtain on modern hardware within seconds an accurate set of eigenvalues for a fairly large variety of reasonably detailed objects. If the given surface or solid has a boundary, generally the Dirichlet boundary condition is applied. If objects with small holes or missing triangles are to be compared, the Neumann boundary condition can be used instead, because the unwanted holes appear to change the Neumann spectrum not as much as in the Dirichlet case.

In order to “show” how the Shape-DNA can help to distinguish many different surfaces the latter technique was applied to a database of 1000 randomly generated B-Spline surface patches [36]. For these patches the first 11 eigenvalues were calculated and stored with the shapes. By using the Euclidean distance of the normalized 11-dimensional vectors of eigenvalues, each patch could be uniquely identified even

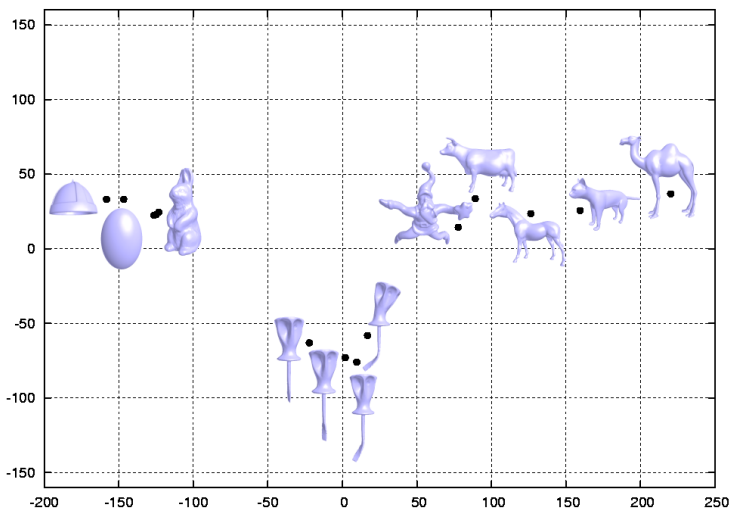


Fig. 10 Clustering of eigenvalues.

with deliberately different (not optimal) meshes introducing distinct calculation errors. Still, these inaccurate eigenvalues yielded distances of less than 0.02 between the original and the modified patch. Furthermore, from all the 500,000 possible pairs of different patches only 300 had a distance of less than 0.3 to each other, none was closer than 0.15. This confirmed the conjecture that the Laplace–Beltrami method is sensitive enough to be used for identifying patches even with reduced capacities for calculation (since only the first 11 eigenvalues were used).

In another experiment, the spectra of different objects were computed and multi-dimensional scaling was employed to obtain the two-dimensional projection in Fig. 10 which shows how similar objects cluster according to their eigenvalues. Of course projecting the high dimensional feature vectors to a very low dimensional space means a massive loss of information, resulting in the formation of additional clusters, and thus cannot serve more than purposes of illustration. For practical applications one should work with more than two dimensions.

Furthermore [36] contains some results with respect to the mutual independence of the eigenvalues and on the rapid convergence of the heat trace series. Especially the latter property made it possible to extract the volume, the boundary length and the Euler characteristic of a shape from its computed eigenvalues with high numerical accuracy. This numerical approach was novel and confirmed the theoretical results stated in (8).

As a biomedical application it was shown later in [28, 38, 39] that Laplace–Beltrami spectra possess the discriminatory power to distinguish two populations of female persons via the shapes of their respective caudate nuclei. In this biomedical application one population would contain normal control subjects while the

other population would consist of subjects with with schizotypal personality disorder. The caudate nucleus of a person is a subcortical gray matter structure of the brain, involved in memory function, emotion processing, and learning.

4.2 Laplace Spectra as Image DNA

In order to use Laplace–Beltrami eigenvalues as fingerprints for images, these images have to be modeled as Riemannian manifolds. For example, a gray scale image can be represented as a surface defined by the graph of a height function being the gray scale intensity function of the image while a color image can be understood as a two-dimensional surface in a five-dimensional Euclidean space whose coordinates include the intensity parameters of the red, green, blue values assigned to any (x, y) pixel of the image. It is possible as well to understand other even higher dimensional signals as height functions and therefore as manifolds, whose Laplace–Beltrami spectra can be computed. These topics were studied by Peinecke during his PhD research.

Another approach pursued by Peinecke was an extension of the classical Laplacian eigenvalue problem (7) to the form

$$-\Delta f = \lambda \rho f$$

in which the gray-value information of an image is encoded in a *mass-density-function* ρ instead of the structure of the representing manifold [31].

Although using the discrete Laplace operator or more generally using eigenvalues of different operators and matrices derived from this operator is a well known and established technique in the community of shape and image recognition, typical applications employ discrete forms of the Laplacian directly instead of making use of the underlying continuous operator. An advantage of the continuum point of view is the independence of the particular discretization employed in the computation, as the results are stable under mesh refinement or change of image resolution.

In a series of example calculations, Peinecke observed that the discrete graph-based Laplace–Kirchhoff and the Laplace–Beltrami operator perform similarly in terms of run time. However, while the Laplace–Kirchhoff operator is more easily implemented, the Laplace–Beltrami variants open up the possibility to use a coarser mesh and thus save computation time. This observation fits into the general finding that for surfaces, images and solids Laplace spectra derived from a discrete model (instead of using the underlying continuous operator) typically have the disadvantage that they make it difficult to decide if two objects are similar when using spectra obtained from different discretizations and different resolutions. In the continuous differential geometric (parametrization invariant) setting the afore-mentioned decision is possible under reasonable assumptions for images, surfaces, solids with or without boundary. Indeed for the latter objects Laplace spectra derived within a continuous (parametrization invariant) setting provide the gold standard and spectra obtained within a merely discrete combinatorial point set setting must be shown to

that in 96% of the cases it was possible to match an image with transformed copies of itself. For a more detailed discussion of the implementation and the results, we refer the reader to [30, 32]. With respect to color images, the proposed methods were shown to be especially useful in the presence of rotations or color rotations, changes of contrast and scale, and combinations of all these operations, since the underlying calculations based on the continuous Laplace–Beltrami operator are invariant against such transformations. It was shown, that the proposed method uses substantially less information than established techniques for discriminating collections of images while maintaining a high reliability. This is especially useful for data bases of images where high dimensional searches are very cost intensive, see for example [7, 8].

5 Conclusions and Prospects

This survey chapter reviewed the contributions of the Welfenlab to GRK 615. All those contributions could essentially be viewed as being partial to a field that one might call “Computational Differential Geometry”. This description would be justified because the respective research essentially presents analysis, discussion and applications of methods that would result in numerical computations of entities that mostly were originally introduced within the classical framework of differential geometry avoiding numerical computations.

The contributions in this chapter are limited to a specific selection of subjects including *Cut Locus*, *medial axis*, *geodesics*, *focal sets*, *conjugate loci*, *geodesic Voronoi diagrams*, *Laplace Spectra of surfaces*, *solids and images*. Despite this limitation the contributions presented in this chapter cover important highlights of research the first author has been involved in since more than 30 years. Many of the mentioned geometric entities that 30 years ago would only exist as mental objects (resulting from mathematical definitions) can nowadays be efficiently numerically computed via works outlined in this chapter. Although those numerical computations are now to some extent possible in a number of relevant situations one should mention that many if not most difficult questions still remain open, see e.g. the remark at the end of Section 2. Certainly the latter point is one of the reasons why various research topics outlined in this chapter (described by the words presented in italics above) being – 20 years ago – initially pursued by a small number of computational researchers only (including computational geometers, computer scientists and engineers) nowadays constitute a substantial part of main stream research in the respective areas. Overall it has turned out that areas that say 25 years ago were viewed at as being sort of exotic in the respective communities – including researchers from computational geometry and computer graphics – mean while are moving into the center of attention in the respective communities. There are several reasons for this development. One is that the area of computational geometry is becoming more and more sophisticated. This holds because the respective researchers are realizing that elementary methods are tentatively exhausted and they are discovering the power

of advanced mathematical tools contained in the theoretical achievements of local and global differential geometry. The other equally or perhaps even more important reason for this development is that sophisticated tools from differential geometry can help to make important progress for the central questions of geometric modeling, computer graphics and image processing. Those central problems are *Shape and Image Cognition* and *(Re)-Construction and Compression* [47]. The application of tools of differential geometry to the afore-mentioned subjects will be the topic of an upcoming paper expanding the referenced keynote lecture [47].

References

1. R. Algaier. Schnelle dynamische Voronoi-Diagramme mit History-DAG. Diplomarbeit, Leibniz Universität Hannover, December 2009.
2. E.L. Allgower and K. Georg. *Introduction to Numerical Continuation Methods*, Classics in Applied Mathematics, Vol. 45, SIAM, 2003.
3. T. Altschaffel. Untersuchungen zur Spektralanalyse von Freiformflächen. Diplomarbeit, Leibniz Universität Hannover, May 1999.
4. N. Amenta and R.K. Kolluri. The medial axis of a union of balls. *J. Computational Geometry*, 20:25–37, 2001.
5. M. Baer. Berechnung Medialer Achsen von einfach berandeten zusammenhängenden Teilstücken parametrisierter Flächen. Diplomarbeit, Leibniz Universität Hannover, December 1998. Available as Wellenlab Report 5.
6. W. Beneker. Rechnergestützte Simulation des Füllverhaltens beim Gesenkschmieden. *Fortschritt-Berichte VDI Reihe*, Vol. 20(187), VDI, 1995.
7. S. Berchtold, C. Böhm, B. Braunnüller, D.A. Keim, and H.-P. Kriegel. Fast parallel similarity search in multimedia databases. In *SIGMOD'97: Proceedings of the 1997 ACM SIGMOD International Conference on Management of Data*, pages 1–12, ACM Press, 1997.
8. S. Berchtold, D.A. Keim, and H.-P. Kriegel. The X-tree: An index structure for high-dimensional data. In T.M. Vijayaraman, A.P. Buchmann, C. Mohan, and N.L. Sarda (Eds.), *Proceedings of the Twenty-Second International Conference on Very Large Data Bases*, Mumbai (Bombay), India, pages 28–39, Morgan Kaufmann Publishers, Los Altos, CA, September 1996.
9. F.R. Biglari, N.P. O'Dowd, and R.T. Fenner. Optimum design of forging dies using fuzzy logic in conjunction with the backward deformation method. *International Journal of Machine Tools and Manufacture*, 38(8):981–1000, August 1998.
10. P. Blanke and F.-E. Wolter. Fast inverse forging simulation via medial axis transform. In *Proceedings of the 2007 International Conference on Cyberworlds, NASAGEM Workshop*, pages 396–403, IEEE Computer Society, Washington, DC, 2007.
11. G. Böttcher. Medial axis and haptics. Diplomarbeit, Leibniz Universität Hannover, October 2004.
12. A.N. Bramley. UBET and TEUBA: Fast methods for forging simulation and preform design. *Journal of Materials Processing*, 116, 2001.
13. T. Culver. Computing the medial axis of a polyhedron reliably and efficiently. PhD Thesis, Department of Computer Science, University of North Carolina, Chapel Hill, 2000.
14. T.K. Dey and W. Zhao. Approximating the medial axis from the Voronoi diagram with a convergence guarantee. *Algorithmica*, 38:179–200, 2004.
15. M.P. do Carmo. *Riemannian Geometry*. Birkhäuser, Boston, 1992.
16. C.B. Garcia and W.J. Zangwill. *Pathways to Solutions, Fixed Points, and Equilibria*. Prentice-Hall, 1984.

17. C. Gordon, D.L. Webb, and S. Wolpert. One cannot hear the shape of a drum. *Bull. Amer. Math. Soc.*, 26:134–138, 1992.
18. H. Naß. Computation of medial sets in Riemannian manifolds. PhD Thesis, Leibniz Universität Hannover, 2007.
19. A. Howind. Untersuchungen und Berechnungen zur Medialen Achse im Raum. Diplomarbeit, Leibniz Universität Hannover, October 1998.
20. T. Howind. Spektralanalyse von berandeten Gebieten. Diplomarbeit, Leibniz Universität Hannover, September 1998.
21. S.M. Hwang and S. Kobayashi. Preform design in disk forging. *International Journal of Machine Tool Design & Research*, 26(3):231–243, 1986.
22. R. Kunze, F.-E. Wolter, and T. Rausch. Geodesic Voronoi diagrams on parametric surfaces. In *Proceedings of CGI'97*, Vol. 6, IEEE Computer Society, 1997. Available as Welfenlab Report 2.
23. H. Mathieu. Ein Beitrag zur Auslegung der Stadienfolge beim Gesenkschmieden mit Grat. *Fortschritt-Berichte VDI-Reihe 2*, 213, VDI, 1991.
24. H.P. McKean and I.M. Singer. Curvature and the eigenvalues of the Laplacian. *J. Diff. Geom.*, 1:43–69, 1967.
25. M. Michael. Konstruktionsbegleitende Modellierung von Schmiedeprozessen. PhD Thesis, Leibniz Universität Hannover, 1999.
26. H. Naß, F.-E. Wolter, C. Doğan, and H. Thielhelm. Medial axis (inverse) transform in complete 3-dimensional Riemannian manifolds. In *Proceedings of the 2007 International Conference on Cyberworlds, NASAGEM Workshop*, pages 386–395, IEEE Computer Society, Washington, DC, 2007.
27. H. Naß, F.-E. Wolter, H. Thielhelm, and C. Doğan. Computation of geodesic voronoi diagrams in 3-space using medial equations. In *Proceedings of the 2007 International Conference on Cyberworlds, NASAGEM Workshop*, pages 376–385, IEEE Computer Society, Washington, DC, 2007.
28. M. Niethammer, M. Reuter, F.-E. Wolter, S. Bouix, N. Peinecke, M.-S. Ko, and M.E. Shenton. Global medical shape analysis using the Laplace–Beltrami-spectrum. In *Proceedings of MIC-CAI07, 10th International Conference on Medical Image Computing and Computer Assisted Intervention*, 2007.
29. N. Obydenna. Implementierung einer Datenstruktur für simpliziale 3D-Netze. Studienarbeit, Leibniz Universität Hannover, April 2009.
30. N. Peinecke. Eigenwertspektren des Laplaceoperators in der Bilderkennung. PhD Thesis, Leibniz Universität Hannover, 2006.
31. N. Peinecke and F.-E. Wolter. Mass density Laplace-spectra for image recognition. In *Proceedings of the 2007 International Conference on Cyberworlds, NASAGEM Workshop*, pages 409–416, IEEE Computer Society, Washington, DC, 2007.
32. N. Peinecke, F.-E. Wolter, and M. Reuter. Laplace-spectra as fingerprints for image recognition. *Computer-Aided Design*, 6(39):460–476, 0 2007.
33. M.M. Postnikov. *The Variational Theory of Geodesics*. Saunders, Philadelphia, PA, 1967.
34. T. Rausch. Analysis and computation of the geodetic medial axis of bordered surface patches (Untersuchungen und Berechnungen zur geodätischen Medialen Achse bei Berandeten Flächenstücken). PhD Thesis, Leibniz Universität Hannover, 1999.
35. T. Rausch, F.-E. Wolter, and O. Sniehotta. Computation of medial curves in surfaces. In *Proceedings of Conference on the Mathematics of Surfaces VII*, pages 43–68, Institute of Mathematics and Applications, 1996. Also available as Welfenlab Report 1.
36. M. Reuter, F.-E. Wolter, and N. Peinecke. Laplace–Beltrami spectra as shape DNA of surfaces and solids. *Computer-Aided Design*, 4(38):342–366, 2006.
37. M. Reuter, S. Biasotti, D. Giorgi, G. Patanè, and M. Spagnuolo. Discrete Laplace–Beltrami operators for shape analysis and segmentation. *Computers & Graphics*, 33(3):381–390, 2009.
38. M. Reuter, M. Niethammer, F.-E. Wolter, S. Bouix, N. Peinecke, M.-S. Ko, and M.E. Shenton. Global medical shape analysis using the volumetric laplace spectrum. In *Proceedings of the 2007 International Conference on Cyberworlds, NASAGEM Workshop*, pages 417–426, IEEE Computer Society, Washington, DC, 2007.

39. M. Reuter, F.-E. Wolter, M. Shenton, and M. Niethammer. Laplace–Beltrami eigenvalues and topological features of eigenfunctions for statistical shape analysis. *Computer-Aided Design*, 41(10):739 – 755, 2009.
40. E.C. Sherbrooke. 3D shape interrogation by medial axis transform. PhD Thesis, Department of Ocean Engineering, MIT, Boston, MA, 1995.
41. H. Thielhelm. Geodätische Voronoi Diagramme. Diplomarbeit, Leibniz Universität Hannover, May 2007.
42. M. Wienströer. Konstruktionsintegrierte Prozesssimulation der Stadienfolge beim Schmieden mittels Rückwärtssimulation. PhD Thesis, Leibniz Universität Hannover, 2004.
43. F.-E. Wolter. Interior metric, shortest paths and loops in Riemannian manifolds with not necessarily smooth boundary. Diplomarbeit, Freie Universität Berlin, 1979.
44. F.-E. Wolter. Distance function and cut loci on a complete Riemannian manifold. *Arch. Math.*, 1(32):92–96, 1979.
45. F.-E. Wolter. Cut loci in bordered and unbordered Riemannian manifolds. PhD Thesis, Technical University of Berlin, 1985.
46. F.-E. Wolter. Cut locus & medial axis in global shape interrogation & representation. MIT Design Laboratory Memorandum 92-2 and MIT National Sea Grant Library Report, 1992. MIT, December 1993 (revised version).
47. F.-E. Wolter. Shape and image cognition, (Re)-construction and compression via tools from differential geometry, Keynote Lecture presented at CGI 2010, Singapore. Available at http://cgi2010.miralab.unige.ch/CGI_InvitedSpeakers.html, 2010.
48. F.-E. Wolter, S. Cutchin, T. Hausman, B. Johnson, S. Goehring, and L. Lambers. Project Riemann source code. Available at <http://www.welfenlab.de/en/research/projects/riemann>, 1988.
49. F.-E. Wolter and K.-I. Friese. Local and global geometric methods for analysis interrogation, reconstruction, modification and design of shape. In *Proceedings of Computer Graphics International 2000*, Geneva, Switzerland, pages 137–151, IEEE Computer Society, 2000. Also available as Welfenlab Report 3.
50. F.-E. Wolter, M. Reuter, and N. Peinecke. Geometric modeling for engineering applications. In E. Stein, R. de Borst, and T.J.R. Hughes (Eds.), *Encyclopedia of Computational Mechanics. Part 1: Fundamentals*, chapter 16, John Wiley & Sons, 2007.
51. G. Xu. Discrete Laplace–Beltrami operators and their convergence. *Computer Aided Geometric Design*, 21:767–784, 2004.